Characterization by X-ray absorption spectroscopy of bimetallic Re-Pd/ TiO 2 catalysts efficient for selective aqueous-phase hydrogenation of succinic acid to 1,4-butanediol

Benoit Tapin, Bao-Khanh Ly, Christine Canaff, Florence Epron, C. Pinel, M. Besson, Catherine Especel

Characterization by X-ray absorption spectroscopy of bimetallic Re-Pd/TiO_2 catalysts efficient for selective aqueous-phase hydrogenation of succinic acid to 1,4-butanediol

Benoît TAPIN[a], Bao Khanh LY[b], Christine CANAFF[a], Florence EPRON[a], Catherine PINEL[b], Michèle BESSON[b], Catherine ESPECEL[a*]

[a]Institut de Chimie des Milieux et des Matériaux de Poitiers (IC2MP), UMR 7285 CNRS-Université Poitiers, 4 rue Michel Brunet, TSA 51106, 86073 Poitiers Cedex 9. France.

**E-mail: catherine.especel@univ-poitiers.fr, Tel: +33(0)549453479*

[b]Univ Lyon, Univ Claude Bernard, CNRS, Institut de recherches sur la catalyse et l'environnement de Lyon (IRCELYON), UMR 5256, 2 avenue Albert Einstein, 69626 Villeurbanne Cedex. France.

Abstract

Re-Pd catalysts supported on TiO_2 (P25 or DT51) prepared by successive impregnation (SI) or by Re deposition on Pd/TiO_2 by catalytic reduction (CR) were characterized by XANES and EXAFS at the Pd and Re edges. These samples were shown to be efficient for the selective hydrogenation in aqueous solution of succinic acid (SUC) to 1,4-butanediol (BDO) (T = 160 °C, P(H_2) = 150 bar). This study clearly highlights the need for *in situ* re-activation of Re-based systems before their characterization or use, since Re species are fully re-oxidized (Re^{7+}) by contact with air. The XANES quantitative analysis at the Re L_{III}-edge reveals that after *in situ* reduction, the Re average reduction state is in most cases inferior or equal to + 3, indicating the presence of a mixture of Re^{3+} and Re^0 species in all reduced catalysts. EXAFS study indicates that the Re species are mainly located at the Pd-support interface for the CR sample, whereas a part of Re entities is also deposited as isolated forms on the support in the case of the SI catalyst. The Re-Pd/DT51-SI system leading to the best BDO yield displays a specific arrangement of the Pd and Re species (Re deposit on Pd sites of high coordination). In this sample, the Re^0 species, present in none negligible proportion, would contribute similarly as Pd metal to the efficient transformation of SUC towards GBL, which is further converted to BDO on sites involving Pd^0 and oxidized Re^{3+} species nearby.

Keywords

Re-Pd catalysts; succinic acid hydrogenation; butanediol; X-ray absorption spectroscopy

Highlights

- Re-Pd/TiO_2 catalysts were characterized by XANES and EXAFS at the Pd and Re edges.
- They were prepared by successive impregnation (SI) or catalytic reduction (CR).
- Re species are fully re-oxidized (Re^{7+}) by contact with air.
- After reduction, the Re average valence state is inferior or equal to + 3.
- Re location around Pd differs according to the preparation way (SI or CR).

Graphical abstract

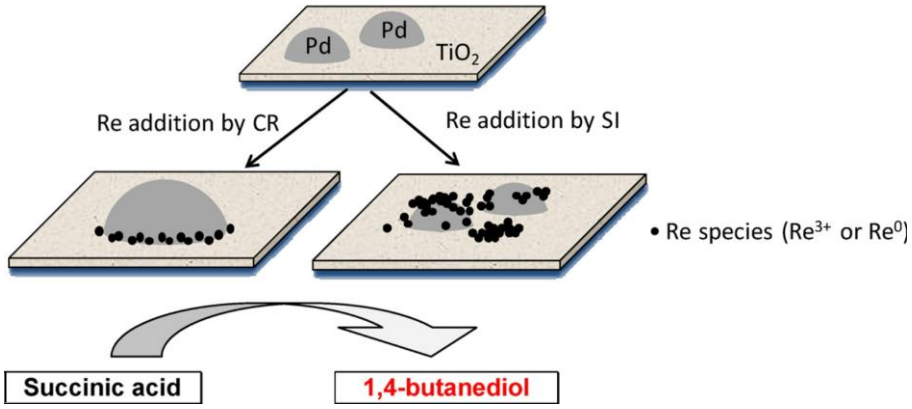

1. Introduction

1,4-butanediol (BDO) is a versatile chemical that can be used in a wide range of industrial applications, as organic solvent or as monomer for production of adhesives, fibers and polyurethanes [1,2]. In the last decade, BDO has received much attention as an important raw material for thermoplastic polymers such as polybutylene terephthalate (PBT) and polybutylene succinate (PBS) [3]. As the use of these polymers is growing fast, the global demand for BDO is expected to increase rapidly. With the development of biorefinery processes, BDO production moves nowadays toward the utilization of sustainable and renewable resources such as biomass, while it was traditionally issued from hydrogenation of maleic anhydride derived from petrochemical feedstocks [4-5]. In this context, conversion of succinic acid (SUC) to BDO by catalytic hydrogenation can be considered as a promising process, since SUC is recognized as one of the promising C_4 platform chemicals that can replace maleic anhydride [2,3,6,7]. As shown in Scheme 1, SUC can be hydrogenated to a first cyclic intermediate *i.e.* γ-butyrolactone (GBL), which is further hydrogenated to BDO or tetrahydrofuran (THF).

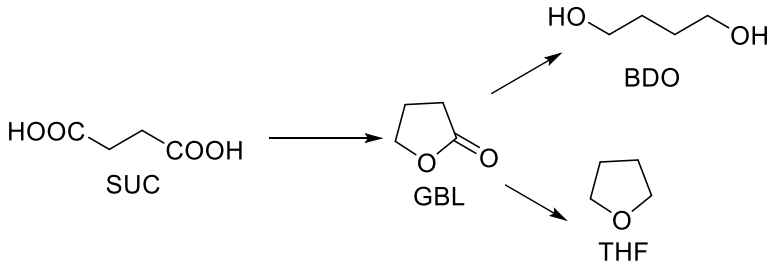

Scheme 1. Catalytic hydrogenation of SUC to BDO.

In order to selectively produce BDO *via* hydrogenation of SUC, several supported metal catalysts have been investigated leading to the following statements: (i) noble metal-based monometallic catalysts such as Rh, Ru and Pd allow mainly converting SUC to GBL [8-11], (ii) noble metal-based bimetallic catalysts such as Pd-Re, Pt-Re or Ru-Re are required to produce selectively BDO from SUC [12-16].

Recently, we have published several papers devoted to the study of Pd/TiO_2 catalysts modified by Re addition in order to optimize the formation of BDO from SUC hydrogenation performed in aqueous phase [13,17-19]. For that purpose, several series of Re-2wt%Pd/TiO_2 catalysts with various Re loadings were prepared from two different TiO_2 supports, by using two procedures for the preparation of Pd/TiO_2 parent monometallic systems and two methods for Re addition (successive impregnation or deposition by catalytic reduction). As reported in

our previous papers, extensive characterizations were performed on all Re-2wt%Pd/TiO_2 bimetallic catalysts series: H_2 chemisorption, X-ray diffraction (XRD), transmission electron microscopy coupled with energy dispersive X-ray spectroscopy (TEM-STEM-EDX), X-ray photoelectron spectroscopy (XPS), temperature programmed reduction (TPR), model reaction of cyclohexane dehydrogenation. For each catalytic system, significant interactions between Pd and Re entities were revealed. From these preliminary results, the active sites involved in the transformation of SUC to GBL then BDO were expected to be at the interface between the closest Pd and ReO_x species. In the present paper, in order to characterize more precisely the structure and interaction of Re species with Pd nanoparticles, we report complementary X-ray absorption spectroscopy (XAS) analysis of these bimetallic catalysts extracted from XANES and EXAFS spectra. On the one hand, the XANES (X-ray Absorption Near Edge Structure) region, corresponding to the part of the X-ray absorption spectrum near the ionization threshold of core electrons, is sensitive to both the electronic structure of the detected absorbing atom (oxidation degree), since the intensity of structures is nearly proportional to the density of the unoccupied states responding to transition rules, and the stereochemical arrangement of neighbors around the absorbing atom [20,21]. On the other hand, the EXAFS (Extended X-ray Absorption Fine Structure) region is an excellent technique for investigating geometric properties of bimetallic nanocatalysts, due to its local structure sensitivity and excellent spatial resolution [22]. With the help of these both techniques, the objective of the present study is to clarify the following points:

(i) previously, the qualitative and quantitative XPS data were supposed to be representative of the whole nanoparticles, from the surface to the bulk of the samples, due to the narrow and homogeneous particle size observed by TEM compared to the depth analyzed by XPS. The determination of the Re average oxidation state by XANES experiments at the Re edge would confirm or not this hypothesis.

(ii) from this XANES analysis, the presence of Re^{3+} species observed in various proportions from XPS data on all bimetallic catalysts will be then comforted or not, this point being crucial for the well understanding of the precise nature of active sites on our catalytic systems.

(iii) Re addition to Pd/TiO_2 catalysts induced a synergetic phenomenon for the SUC hydrogenation reaction, however, all bimetallic catalysts did not display the same BDO yield. The localization of the Pd and Re atoms relative to each other, deduced from EXAFS analysis at the edge of each metal could allow understanding the differences in the catalytic performances observed as a function of the preparation method and the type of TiO_2 support.

2. Experimental

2.1. Monometallic and bimetallic catalysts preparation

Three monometallic 2wt%Pd_{Cl}/P25, 2wt%Pd_{KCl}/P25 and 2wt%Pd_{KCl}/DT51 catalysts were prepared on TiO_2 P25 (Degussa-Evonik, 50 m^2 g^{-1}) or TiO_2 DT51 (Cristal, 88 m^2 g^{-1}), either by impregnation of $PdCl_2$ precursor salt in acidic aqueous solution (noted Pd_{Cl}) or by deposition-precipitation using K_2PdCl_4 as the precursor (noted Pd_{KCl}), as described in details in a previous reference [11]. Each sample was reduced under H_2 flow at 300 °C and passivated at room temperature (RT) in 1 % v/v O_2/N_2 for 30 min (except the Pd_{Cl}/P25 catalyst which was not passivated, but exposed to air directly after N_2 flushing, following the procedure applied in the laboratory in charge of this preparation within the work consortium). Two monometallic 2wt%Re/P25 and 3.1wt%Re/DT51 catalysts were also synthesized by impregnation on the support of an aqueous solution of ammonium perrhenate, NH_4ReO_4, adjusted to pH 1 with HCl only for 2wt%Re/P25. After evaporation of the solvent and drying in an oven at 120 °C, monometallic Re solids were reduced at 450 °C in H_2, passivated at RT in 1 % v/v O_2/N_2 for 30 min in the case of the Re/DT51 sample, and contacted with air after N_2 flushing at RT [18].

Four series of bimetallic catalysts (two supported on P25 and two on DT51) were prepared by addition of various amounts of Re from aqueous solution of NH_4ReO_4 on the parent 2wt%Pd_{Cl}/P25, 2wt%Pd_{KCl}/P25 or 2wt%Pd_{KCl}/DT51 catalyst, respectively, and using either successive impregnation (SI) or deposition by catalytic reduction (CR), as described elsewhere [13,17,18]. Briefly, in the SI procedure, an aqueous solution of a predetermined amount of the Re salt was added to a suspension of the Pd/TiO_2 catalyst at RT during 5 h, then the excess water was evaporated under vacuum for 30 min, and the solid was dried overnight at 50 °C under vacuum. After reduction in H_2 flow at 450 °C, the SI catalysts were passivated at RT in 1 % v/v O_2/N_2 for 30 min, and stored in a flask under Ar. The CR deposition method is based on a surface redox reaction between adsorbed atomic hydrogen on Pd (Pd-H_{ads}) of the parent catalyst and the Re oxidized species of the precursor according to the overall reaction: ReO_4^- + n Pd-H_{ads} + (8-n) H^+ → $(Pd)_n$-$Re^{(7-n)+}$ + 4 H_2O. In the CR procedure, the parent Pd catalyst placed in a fixed-bed reactor was activated under a flow of H_2 at 300 °C. After cooling, the Re solution (acidified with HCl at pH 1 and degassed) was poured onto the Pd/TiO_2 catalyst and the mixture was maintained for 1 h under H_2 bubbling. After filtration, the solid was dried under H_2 and reduced at 450 °C, then allowed to cool down to RT and slowly exposed to air after N_2 flushing. The catalysts prepared by CR were stored in ambient air. It can be noticed that the reduction temperature of the catalysts was

adapted to the metal, knowing palladium oxides are reduced at low temperature (< 300 °C) whereas rhenium oxides require higher temperatures to start to be reduced [18].

2.2. X-ray absorption spectroscopy (XAS)

XAS experiments were carried out on the SAMBA (Spectroscopies Applied to Materials Based on Adsorption) beamline at the SOLEIL Synchrotron (Saint Aubin, France). The SOLEIL storage ring was operated at 2.75 GeV with a ring current of about 500 mA. The XAS data were obtained in the transmission mode at the Re L_I- and L_{III}-edges (12.527 keV and 10.535 keV, respectively) and the Pd K-edge (24.350 eV).

The catalysts were placed between two carbon slabs in a cell designed for *in situ* XAS analysis under flowing gas at elevated temperature, displaying a surface of 0.4 cm^2 (0.8 cm * 0.5 cm) and a thickness of 0.4 cm. All samples were reduced *in situ* in the XAS cell according to the following procedure: ① N_2 purge at RT; ② 5%H_2/Ar flow (60 mL min^{-1}) at RT; ③ temperature ramp (5 °C min^{-1}) under 5%H_2/Ar; ④ temperature maintenance under 5%H_2/Ar at 300 °C (monometallic Pd) or 450 °C (monometallic Re and bimetallic Re-Pd); ⑤ cooling under 5%H_2/Ar flow to 30 °C. Spectra were recorded throughout this protocol and merged in the case of steps ①, ② and ⑤ performed at a fixed temperature.

The XAS data were processed using the Athena software [23] for spectral averaging, background removal, post-edge normalization, and XANES analysis at the Re-edges. The Re oxidation states in the monometallic Re and bimetallic Re-Pd samples were determined by comparing the inflection point of the Re L_{III}-edge from a given sample to the inflection point of standards with known Re oxidation state. The EXAFS spectra at the Pd K-edge and Re L_{III}-edge were analyzed using Artemis software [23], which implemented FEFF [24]. The normalized EXAFS data were appropriately k-weighted and then Fourier transformed from k-space (in the range 3-12 $Å^{-1}$) to the R-space using a Hanning window sill to obtain a radial distribution function |F(R)|. The inversely Fourier filtered data were fitted in R-space using single scattering Pd-Pd (or Re-Re), Pd-Cl (or Re-Cl), Pd-O (or Re-O) and Pd-Re generated theoretically using FEFF code extracted from ATOMS [25].

Re metal powder (Alfa Aesar, 99.99 %), $ReCl_3$ (Aldrich, 99.9 %), ReO_2 (Alfa Aesar, 99.9 %), ReO_3 (Aldrich, 99.9 %), Re_2O_7 (Aldrich, 99.995 %) and NH_4ReO_4 (Aldrich, > 99 %) were used as references for Re 0, +3, +4, +6 and +7 oxidation states, respectively. A Pd foil supplied by the SAMBA beamline team, and pressed powders of PdO (Alfa Aesar, 99.9 %) and $PdCl_2$ (Alfa Aesar, 99.99 %) were used as standards for analyzes at the Pd K-edge. The spectra of all these references were recorded at RT. Amplitude-reduction factors S_0^2 for Pd

and Re, both equal to one, were determined from fitting the first shell EXAFS of Pd foil and Re powder.

2.3. SUC hydrogenation

The hydrogenation reaction of succinic acid (SUC) was carried out in aqueous-phase at 160 °C under 150 bar of hydrogen pressure in a 300 mL high-pressure batch reactor (Parr Instrument 4560, Hastelloy C276) equipped with a magnetically driven impeller (1200 rpm) and a liquid sampling system described previously [12-14]. The reactor was loaded with 120 g of a 5 wt% SUC aqueous solution and 1 g of catalyst (molar ratio SUC/Pd ca. 250). After purging with Ar, the reactor was heated under Ar to 160 °C, then H_2 was adjusted to 150 bar which corresponded to time zero. Quantitative analyses of liquid samples withdrawn from the reactor at regular intervals were performed using both a Shimadzu high performance liquid chromatography instrument (equipped with an ICSEp Coregel 107H column and a differential refractometer and a UV detection in series), and a gas chromatography (equipped with a HP-5 column) as previously described [11-14,17,18]. The carbon mass balance in liquid phase was measured by evaluating total organic carbon (TOC) using a Shimadzu TOC-V_{CSH} analyzer.

3. Results and discussion

3.1. Preliminary description of the studied catalysts

As mentioned in the introduction, several series of Re-2wt%Pd/TiO_2 catalysts with various Re loadings, prepared by SI or CR method from two TiO_2 supports (named DT51 and P25) and two Pd precursor salts ($PdCl_2$ noted Pd_{Cl}, and K_2PdCl_4 noted Pd_{KCl}), were previously synthesized and studied in details notably by TEM and XPS [13,17-19]. The main information and characteristics of these catalysts are gathered in Table 1, *i.e.* the nomenclature of each sample, their preparation mode, their chlorine content, the catalytic performances of the best sample of each series, the average metallic particle size and the Re valence state determined by TEM and XPS, respectively, and an estimation of the location of Re and Pd species in relation to each other on the bimetallic catalysts. During SUC reaction performed at 160 °C under 150 bar of H_2 pressure, three main products were observed corresponding to γ-butyrolactone (GBL), the first cyclic intermediate, 1,4-butanediol (BDO, the targeted product) or tetrahydrofuran (THF) (Scheme 1). Traces (1 %) of other products (n-butyric acid, n-butanol and n-propanol) were also detected.

It was highlighted that all Pd/TiO_2 monometallic catalysts gave mainly GBL with no further conversion upon prolonged reaction times, whereas the incorporation of Re (by both SI and

CR procedures) made the hydrogenation of GBL to BDO possible and led to high yield of BDO (reaching up to 90 % for some catalysts series after optimization of the Re content) [13,14,17,18].

Table 1. Main characteristics of Re-2wt%Pd/TiO_2 bimetallic catalyst series prepared by CR (deposition by catalytic reduction) and SI (successive impregnation) methods, and of 2wt%Pd/TiO_2 and 2wt%Re/TiO_2 monometallic catalysts. (Information extracted from previous references)

Catalysts /TiO_2	Pd salt	Synthesis method	Cl content (wt%)	Max. yield to BDO (%)[a]	Main characteristics of reduced samples[b]	Ref.
BIMETALLIC						
Series 1 Re-Pd_{Cl} /P25-CR	$PdCl_2$	CR	0.2	~ 50 % for 0.9 and 1.7wt%Re	đ = 5.3 nm Re^{3+} (100 %) species mainly located at the Pd-support interface	[17] [18]
Series 2 Re-Pd_{KCl} /P25-SI	K_2PdCl_4	SI	< 0.1	~ 65 % for 2.6 and 3.6wt%Re	Re^{3+} (66 %) + Re^0 (34 %) species located on Pd particles and the support	[13] [18]
Series 3 Re-Pd_{KCl} /DT51-CR	K_2PdCl_4	CR	0.5	~ 55 % for 0.8wt%Re	đ = 1-3 nm Re^{3+} (70 %) + Re^0 (30 %) species inhomogeneously deposited due to experimental limitations[c]	[13] [18]
Series 4 Re-Pd_{KCl} /DT51-SI	K_2PdCl_4	SI	0.3	80-90 % for 2.6 and 3.4wt%Re	đ = 1-2 nm Re^{3+} (73 %) + Re^0 (27 %) species located on the Pd particles and the support	[13] [18]
MONOMETALLIC						
Pd_{Cl}/P25	$PdCl_2$	-	0.4	< 5 %	đ = 1.8 nm Pd^0 (100 %)	[18]
Pd_{KCl}/P25	K_2PdCl_4	-	< 0.1	< 5 %	-	
Pd_{KCl}/DT51	K_2PdCl_4	-	< 0.1	< 5 %	đ = 2.4 nm Pd^0 (95 %) + Pd^{2+} (5 %)	[18]
Re/P25	-	-	0.4	< 1 %	đ < 0.7 nm Re^{3+} (85 %) + Re^0 (15 %)	[18]
Re/DT51	-	-	< 0.1	< 1 %	đ < 0.7 nm	[18]

[a] Reactions conditions: 6 g SUC in 114 g water, P_{H2} = 150 bar, T = 160 °C, 1 g catalyst, 48 h reaction time

[b] Average metallic particle diameter determined by TEM (and H_2 chemisorption in the case of the monometallic catalysts), and chemical state determined by XPS after *in situ* reduction in the XPS chamber

[c] The very fine granulation of the DT51 support caused plugging of the frit of the reactor used for the CR preparation method, leading to an inhomogeneous hydrogen flow limiting the catalytic reduction process

As discussed in depth in ref [18], the activation of GBL in water may occur on protonated Re species bound to Pd atoms implying both the carbonyl group and the oxygen in the cycle and

leading to an ester intermediate, which is further hydrogenated over Pd^0 sites to yield BDO (Scheme 2). The active sites are then expected to be at the interface between closest Pd and ReO_x species. In each case, the extensive characterization of the Re-2wt%Pd/TiO_2 bimetallic catalysts series revealed significant interactions between Pd and Re entities. For the most performant systems, XPS analyses highlighted the presence of Re^{3+} and Re^0 species on the surface of the reduced catalysts in various proportions according to the catalysts series (Table 1). These analyses were performed using values of binding energies referenced in literature as well as experimental data extracted from $ReCl_3$ standard compound.

The complementary XAS analyses reported in this paper were performed on representative samples extracted from these catalysts series, *i.e.*: the four bimetallic catalysts 1.7wt%Re-Pd_{Cl}/P25-CR (noted afterward Re-Pd_{Cl}/P25-CR), 2.7wt%Re-Pd_{KCl}/P25-SI (noted afterward Re-Pd_{KCl}/P25-SI), 1.9wt%Re-Pd_{KCl}/DT51-CR (noted afterward Re-Pd_{KCl}/DT51-CR), and 2.6wt%Re-Pd_{KCl}/DT51-SI (noted afterward Re-Pd_{KCl}/DT51-SI), as well as the two monometallic catalysts Pd_{Cl}/P25 and Pd_{KCl}/DT51, and the two monometallic catalysts Re/P25 and Re/DT51.

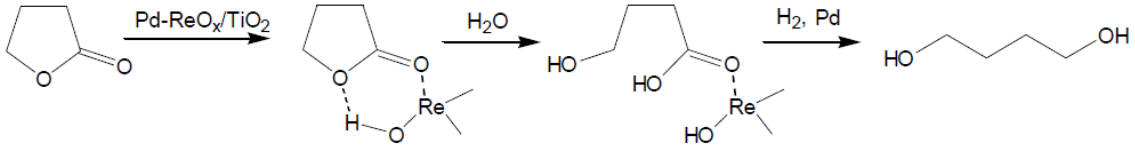

Scheme 2. Schematic reaction pathway to BDO (extracted from [18]).

3.2. Study of the Re oxidation state by XANES

The XANES region (absorption edge position and white line (resonance) intensity) is sensitive to both the electronic structure of the absorbing atom and the stereochemical arrangement of their neighbors [20,21]. Figs. 1a and 1b show the Re L_I and Re L_{III} spectra, respectively, corresponding to the different Re salts used as references, and compared with the Re metal. It can be observed that the edge position shifts to higher energies as the formal oxidation state increases from metallic to oxidized states. At the Re L_I-edge, an important pre-edge at around 12.535 keV is observed in the case of the NH_4ReO_4 and Re_2O_7 compounds, typical of materials for which the Re absorbing atoms do not correspond to a center of symmetry. For ReO_3, ReO_2, $ReCl_3$ and Re metal, there is only a small shoulder at this energy. At the Re L_{III}-edge, spectra are less structured and display a high white line, that shifts sharply towards higher energies with the increase of the oxidation state of Re.

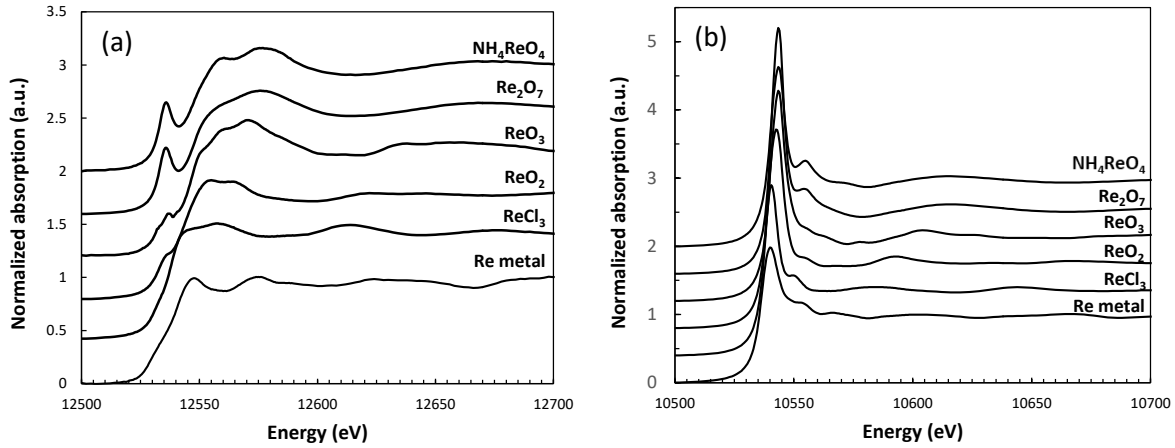

Fig. 1. Spectra of the different Re salts compared with the Re metal obtained at (a) Re L_I-edge and (b) Re L_{III}-edge

For both Re/TiO_2 monometallic catalysts, the evolution of the Re L_I- edge spectra during each step of the *in situ* reduction protocol of the samples in the XAS cell (described in details in section 2.2) is given in Fig. 2. In both cases (P25 and DT51 support), the catalysts prepared-activated-stored and then exposed to N_2 at RT in the beamline exhibit a spectrum with the pre-edge typical of the Re +VII references (NH_4ReO_4 or Re_2O_7). Consequently, the exposure to air of the monometallic Re/TiO_2 catalysts during their storage and transfer to the XAS cell involves a full re-oxidation of the Re species. This assessment was also established by Bare *et al.* who described an extensive study of supported rhenium catalysts by experimental (XAS, STEM, TPR and XPS) and theoretical (DFT) characterizations [26]. They clearly highlighted the need for *in situ* characterization of their reduced catalysts since the reduced Re species were readily reoxidized after the exposure to ambient atmospheric conditions. During the rise in temperature under H_2, the pre-edge disappears leading to XANES profiles after *in situ* reduction getting closer to the $ReCl_3$ or Re metal references. This result is consistent with the XPS analysis previously performed (Table 1) that indicated the presence of a mixture of Re^{3+} (85 %) and Re^0 (15 %) on the Re/P25 sample after reduction.

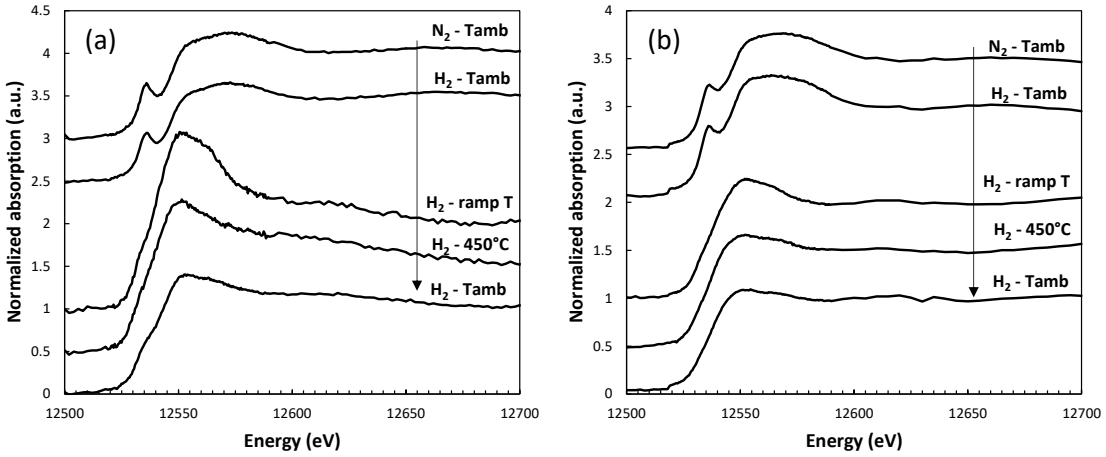

Fig. 2. Spectra at the Re L_I-edge of the two monometallic Re/TiO_2 catalysts at each step of the *in situ* reduction protocol: (a) P25 support and (b) DT51 support.

Fig. 3 gives the XAS profiles of the four studied $Re\text{-}Pd/TiO_2$ bimetallic catalysts, prepared either by CR or SI protocol, supported either on P25 (Fig. 3a) or DT51 (Fig. 3b), and obtained after their *in situ* reduction in the beamline. In the same way as for the Re monometallic samples, the spectra obtained in each case reveal an absorption structure that is intermediate between the profiles of the $ReCl_3$ or Re metal references.

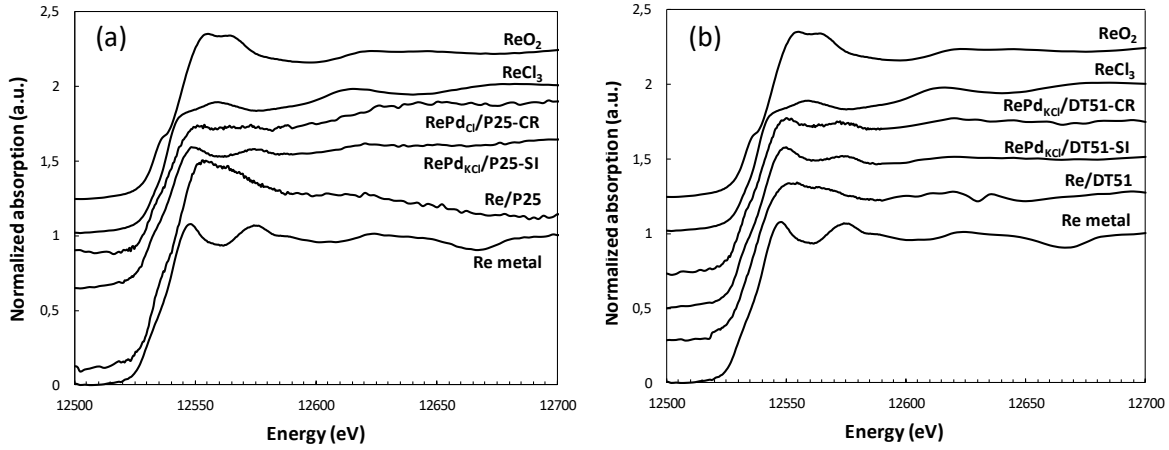

Fig. 3. Spectra at the Re L_I-edge of the $Re\text{-}Pd/TiO_2$ and Re/TiO_2 catalysts after *in situ* reduction at 450°C (spectra taken under H_2 at RT) compared with references.
(a) P25 support and (b) DT51 support.

In order to better estimate the average oxidation state of Re species in the catalysts, the precise position of the Re L_{III}-edge was determined by identification of the inflection point in the white line deduced from the maximum of the first derivative [21,27-29]. From the spectra of Re references, a linear correlation was established between the relative shift of the edge *versus* the one of the Re metal reference, and the Re oxidation state (Fig. 4). From this linear

regression straight line, the average oxidation state was evaluated for all studied catalysts at the various steps of the *in-situ* reduction protocol in the XAS cell (Table 2).

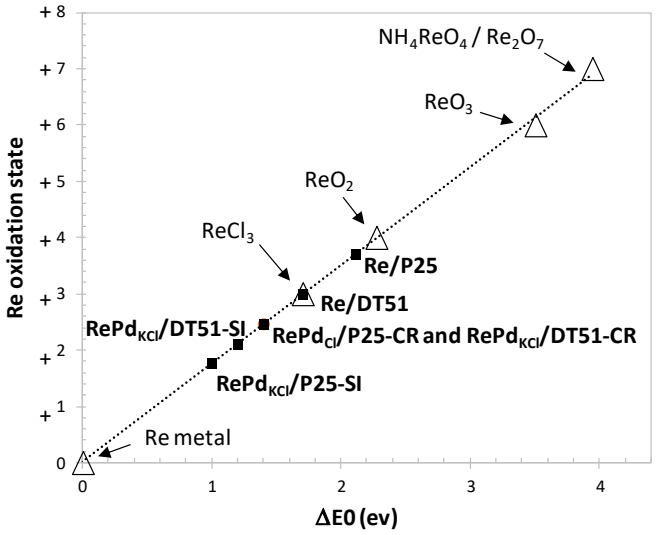

Fig. 4. Correlation of the Re L_{III}-edge energy (inflection point) to the oxidation state of references compounds (triangles) and studied catalysts (black squares) after their *in situ* reduction.

Table 2. Average oxidation state of Re determined at the L_{III}-edge for the monometallic and bimetallic catalysts at each step of the *in situ* reduction protocol[a] (values of oxidation state determined previously by XPS [18] are given for comparison)

Catalysts	**①[a] N_2-RT**	**XPS[b] before red.**	**②[a] H_2-RT**	**③[a] H_2-100°C**	**③[a] H_2-200°C**	**⑤[a] H_2-30°C**	**XPS[c] after red.**
Re/P25	+ 7.0	+ 6.1	+ 7.0	+ 7.0	+ 3.9	+ 3.7	+ 2.6
Re-Pd_{Cl}/P25-CR	+ 6.8	+ 6.5	+ 3.5	+ 3.1	+ 2.5	+ 2.5	+ 3.0
Re-Pd_{KCl}/P25-SI	+ 6.7	+ 5.9	+ 4.0	+ 3.9	+ 3.3	+ 1.8	+ 2.0
Re/DT51	+ 6.8	-	+ 6.8	+ 6.8	+ 3.5	+ 3.0	-
Re-Pd_{KCl}/DT51-CR	+ 7.2	-	+ 4.0	+ 3.9	+ 3.3	+ 2.5	+ 2.1
Re-Pd_{KCl}/DT51-SI	+ 7.2	+ 6.1	+ 3.7	+ 3.5	+ 3.0	+ 2.1	+ 2.2

[a] ① N_2 purge at room temperature (RT); ② 5%H_2/Ar flow at RT; ③ during the temperature ramp under 5%H_2/Ar until 450 °C (spectra taken at 100 °C or 200 °C); ⑤ under 5%H_2/Ar flow after heating at 450 °C and then cooling to 30 °C

[b] XPS analysis of the $Re4f_{7/2}$ component performed on samples after exposure to air

[c] XPS analysis of the $Re4f_{7/2}$ component performed on samples after their *in situ* reduction in the XPS chamber

Firstly, results reported in Table 2 (step ① under N_2-RT) clearly show that after the preparation, reduction and exposure to air, all catalysts (monometallic and bimetallic) display totally oxidized Re species (average oxidation degree near + 7). Based on XAS analyses, Daniel *et al.* observed also that Re in Pt-Re/C bimetallic samples can be fully oxidized (Re^{7+}) in air [27]. As observed in Table 2, the oxidation degrees previously determined by XPS analysis [18] for each Re-Pd/TiO_2 system before their *in situ* reduction were systematically

lower than by XAS, due to a possible partial reduction of the samples under the ultra-high vacuum applied in the XPS analysis chamber (10^{-9} mbar) and perhaps to the fact that XPS data are not totally representative of the whole nanoparticles of the samples as considered in [18], contrary to XAS analysis. Once the N_2 atmosphere is replaced by H_2 flow in the XAS cell at RT (Table 2, step ②), the reduction of the Re species starts whatever the Re-Pd bimetallic catalyst, whereas the oxidation state remains unchanged (near + 7) in both Re monometallic samples. The degree of Re reduction on bimetallic samples evolves very little during the temperature ramp up to 100 °C, then it intensifies between 100 and 200 °C (Table 2, step ③). For the Re-Pd_{Cl}/P25-CR catalyst, the reduction rate seems higher before 200 °C than for the other bimetallic catalysts. Also, reduction is finished at this temperature, since the average oxidation state did not change subsequently, *i.e.* after reduction at 450 °C and cooling down to 30 °C (Table 2, step ⑤). In the case of the monometallic Re/TiO_2 catalysts, the reduction of the Re species finally starts after 100 °C. All these results are totally consistent with the profiles obtained during temperature programmed reduction (TPR) experiments performed on the oxidized catalysts and reported in our previous paper [18], *i.e.* (i) a main hydrogen consumption from 25 °C to 40 °C for all bimetallic catalysts, (ii) not any other consumption at higher temperature in the case of the Re-Pd_{Cl}/P25-CR catalyst, considered as not displaying isolated Re entities on the support, and (iii) a consumption peak at higher temperature, located between 230-450 °C for the Re/P25 sample and before 380°C in the case of the other bimetallic catalysts (Re-Pd_{KCl}/P25-SI, Re-Pd_{KCl}/DT51-CR and Re-Pd_{KCl}/DT51-SI). However, one can note that the comparison between TPR and XAS analyses can be only qualitative. Indeed, a 1%H_2/Ar gas mixture was employed for TPR compared to a 5%H_2/Ar flow for the *in situ* reduction in the XAS cell, and the gas hourly space velocities (GHSV) are completely different, which can explain some little changes in the reduction rates [28]. Finally, at the end of the *in situ* reduction protocol at 450 °C (Table 2, step ⑤, under H_2 at 30 °C), the Re L_{III}-edge energy for Re/DT51 is similar to that of $ReCl_3$ (Fig. 4), which reinforces the existence of Re^{3+} entities from the surface to the bulk of the sample. This oxidation state was also observed for Re species in Ir-ReO_x/SiO_2 catalysts studied by Tomishige's group [28,30-32]. In fact, the oxidation state Re^{3+} is not known to exist as a stable Re_2O_3 oxide, and then is not among the most usual oxidation states for Re, but it has been reported in metal complexes [33,34]. For all bimetallic catalysts, the Re average oxidation states are inferior to + 3. Finally, except for the Re/P25 sample (+ 3.7), the values determined from XANES (Table 2) confirm the exclusive presence of Re^{3+} and Re^0 species in various proportions in all reduced catalysts highlighted by XPS analysis. Moreover, Re species appear more reducible

in the bimetallic catalysts compared to the monometallic ones, leading to the following order of the catalysts according to their respective final oxidation state as shown on Fig. 4: Re-Pd_{KCl}/P25-SI (+ 1.8) < Re-Pd_{KCl}/DT51-SI (+ 2.1) < Re-Pd_{Cl}/P25-CR = Re-Pd_{KCl}/DT51-CR (+ 2.5) < Re/DT51 (+ 3.0) < Re/P25 (+ 3.7). These values are quite close to those calculated from XPS. The largest disparity is observed for the Re/P25 catalyst (+ 3.7 against + 2.6 from XPS), which displays very small particles (size < 0.7 nm) that appear more reduced after the *in situ* reduction performed under pure H_2 in the XPS pretreatment chamber. For a given TiO_2 support (P25 or DT51), the Re oxidation state is systematically lower on the bimetallic sample prepared by the SI method compared to the CR one. In their study devoted to Pt-Re/C samples, Daniel *et al.* observed also a partial reduction of Re species by H_2 while they were fully oxidized in air, but only in the case of bimetallic catalysts and not for the Re/C system [27]. These authors considered that Re remains oxidized on the Re/C catalyst because Re is nearly atomically dispersed on the carbon, whereas the association of Re with Pt in the bimetallic particles allows the reduction after treatment in H_2. Likewise on Pd-Re/C catalysts, Shao *et al.* demonstrated that Pd can significantly promote the reduction of rhenium oxide [35]. Previously, among the four bimetallic catalysts series, we identified that the catalysts exhibiting the best performances in terms of BDO yield in SUC hydrogenation were the bimetallic samples prepared by the SI method (BDO yield at 48 h: 80-90 % for Re-Pd_{KCl}/DT51-SI, ~ 65 % for Re-Pd_{KCl}/P25-SI). For both series of samples, the Re oxidation state obtained after reduction is the smallest, close to + 2.0, indicating the presence of none negligible proportion of Re^0 combined to Re^{3+} species. In the same way as Pd metal, the Re^0 species would contribute efficiently to the transformation of SUC towards GBL, as highlighted by Di *et al.* on Re/C catalysts prepared by microwave-assisted thermolytic method using $Re_2(CO)_{10}$ precursor and displaying well-dispersed metal nanoparticles on support [36]. The GBL molecules formed can be further converted to BDO on sites associating Pd^0 and oxidized Re species.

In conclusion, this XAS study clearly highlights the need for *in situ* reduction of Re-based catalysts before their use, in order to avoid the presence of inactive Re^{7+} entities and limit the metal leaching phenomenon during the catalytic test resulting from the unstable behavior of such species in aqueous phase [19]. The XANES analysis at the Re edge corroborates, on the whole, the data derived previously from XPS before and after *in situ* reduction of the samples. Consequently, our hypothesis considering that the XPS surface technique was representative of the bulk of the studied samples due to their small particle size was correct.

3.3. EXAFS analysis

3.3.1. Pd K-edge analysis

Fourier transforms (FTs) of the Pd K-edge EXAFS analysis of Pd_{Cl}/P25 and Pd_{KCl}/DT51 monometallic catalysts are shown in Fig. 5 at three steps of the *in situ* reduction procedure: step ① under inert gas (N_2) before reduction, step ② before reduction under H_2, and step ⑤ after reduction at RT under H_2. FTs of standard compounds (Pd foil and PdO) extracted in the same k range (3-12 $Å^{-1}$) are also given for comparison. The quantitative data determined by fitting spectra for both monometallic catalysts at steps ① and ⑤ are gathered in Tables 3 and 4, respectively, especially the coordination numbers (CN) and interatomic distances (R). The CN and R values associated to each first Pd coordination shell in the used references are the followings: Pd foil CN(Pd-Pd) = 12, R = 2.75 Å; $PdCl_2$ CN(Pd-Cl) = 4, R = 2.31 Å; PdO CN(Pd-O) = 4, R = 2.02 Å.

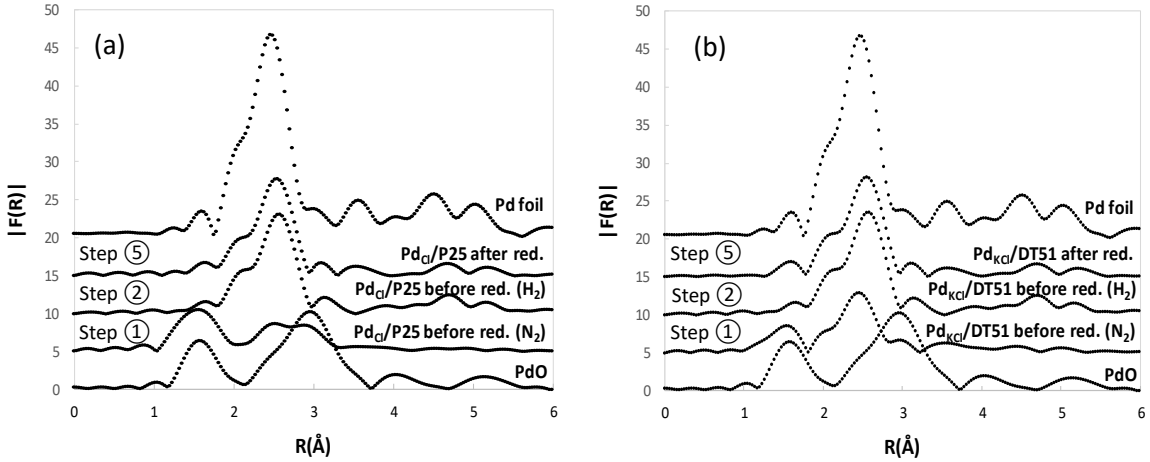

Fig. 5. Magnitude of the Fourier transforms of the k^3-weighted Pd K-edge EXAFS of the monometallic Pd catalysts before and after *in situ* reduction (red.), compared with standard compounds (Pd foil and PdO): (a) Pd_{Cl}/P25 and (b) Pd_{KCl}/DT51.

Before introduction of the H_2 flow and reduction (step ①), Pd species of the monometallic samples are clearly oxidized, as shown by the presence of a noticeable peak between 1-2 Å on the FTs, arising from a Pd-O shell. The oxidation is more pronounced for the Pd_{Cl}/P25 catalyst compared to Pd_{KCl}/DT51 with more O atoms in the neighborhood of Pd atoms, *i.e.* CN (Pd-O) = 2.1 versus 1.7 (Table 3). Given that the average metal particle sizes determined previously by TEM and H_2 chemisorption were quite comparable on both samples (around 2.0 nm, Table 1) [18], this disparity cannot be due, in all likelihood, to a distinct contribution of the oxygen neighbors from the TiO_2 support. It is possible that this difference results from the protocols undergone by each sample at the end of their preparation: after the reductive treatment, Pd_{Cl}/P25 was stored directly under air, whereas Pd_{KCl}/DT51 was passivated under 1

% v/v O_2/N_2 for 30 min, thus allowing it to keep globally a more important metallic character, as proven by its much higher CN (Pd-Pd) compared with Pd_{Cl}/P25. The presence of Pd particles with different morphologies may also explain this difference: for example metallic particles with a flatter shape (raft configuration) in the case of Pd_{Cl}/P25 could lead to a higher metal-support interaction on this catalyst compared to Pd_{KCl}/DT51, and then to a more oxygenated neighborhood. This higher interaction could also favor the presence of residual chlorine *via* oxichlorinated species on Pd_{Cl}/P25 sample. Indeed, it should be mentioned that in the case of this catalyst, a coordination shell with some Cl atoms was introduced to improve the fit, since 0.4 wt% Cl was analyzed on this sample *versus* no Cl content on the Pd_{KCl}/DT51 catalyst (Table 1). The presence of Cl atoms in Pd_{Cl}/P25 originates from the use of a chlorinated salt for the Pd precursor and of hydrochloric acid (to adjust the pH of the impregnation medium) [37].

After replacement of N_2 flow by a H_2 flow, and even before increasing the temperature in the XAS cell (step ②), the peak assigned to the oxygen neighbors decreases significantly for both monometallic catalysts (Fig. 5), and the radial distribution profiles do not evolve anymore until the end of the reduction (step ⑤). These results indicate that the Pd phase of these systems is totally reduced at RT under dihydrogen, as confirmed by the quantitative data in Table 4. As an example, curve fits associated with the results in Table 4 after *in situ* reduction are given in Fig. 6 in the case of the Pd_{Cl}/P25 catalyst. After *in situ* reduction, the neighborhood of the Pd atoms is finally similar for both monometallic catalysts (CN (Pd-Pd) = 6.1) since they display identical spectra. This similarity is quite logical according to the average metal particle size of these two samples determined previously by TEM and H_2 chemisorption (Table 1 [11,18]), which revealed the presence of small metallic Pd nanoparticles (around 2.0-3.0 nm). Consequently, it is likely that the morphology of the Pd particles after reduction is quite comparable on the two monometallic catalysts, with a change of the raft configuration assumed previously on Pd_{Cl}/P25 exposed to air towards a more classical cuboctahedral shape.

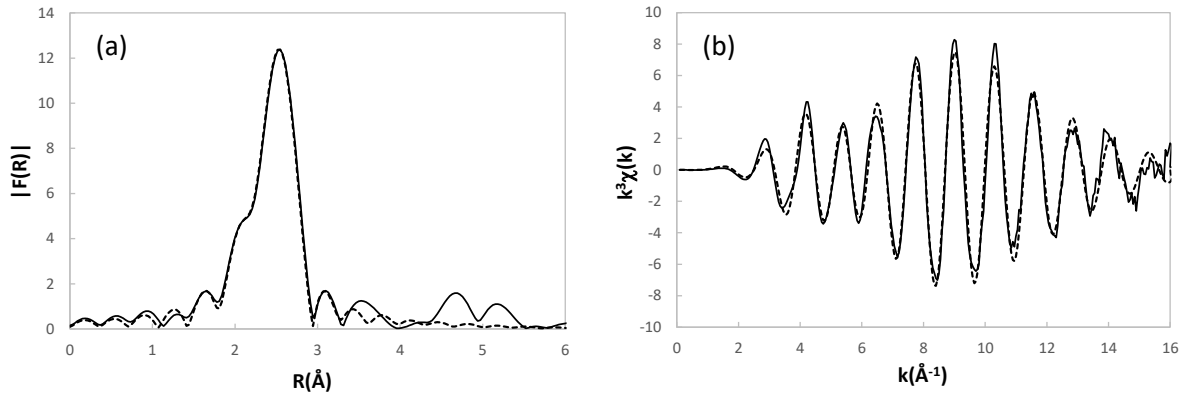

Fig. 6. Comparison of curve fit (dashed line) to experimental data (solid line) from Pd K-edge EXAFS of the monometallic Pd_{Cl}/P25 catalyst after the *in situ* reduction.
(a) Fourier transform and (a) back transform.

Fourier transforms (FTs) of the Pd K-edge EXAFS analysis of the four Re-Pd bimetallic catalysts previously studied by XANES and prepared either by catalytic reduction (CR) or successive impregnation (SI) on P25 and DT51 support are shown in Figs. 7a and 7b, respectively. They are compared with those of the corresponding Pd monometallic samples, before reduction while under inert gas (step ①, Figs 7a-1 and 7b-1) and after *in situ* reduction under H_2 (step ⑤, Figs 7a-2 and 7b-2). For each catalyst, the curve fitting quantitative data at steps ① and ⑤ are gathered in Tables 3 and 4, respectively. A $Pd_{0.88}Re_{0.12}$ alloy (only alloy referenced in HighScorePlus software (reference code 98-010-5663), cubic crystal system with space group Fm-3m, and unit-cell parameters a = b = c = 3.66 Å) was used as standard for fitting the Re coordination shell (R(Pd-Re) = 2.59 Å). It must be noticed that the Pd-Re fcc phase exhibits a smaller lattice parameter compared with Pd fcc structure (3.66 Å *vs* 3.90 Å). This contraction in lattice parameter results in a shorter interatomic distance Pd-Re than in pure Pd metal as already reported by Meitzner *et al.* [38] and Malinowski *et al.* [39].

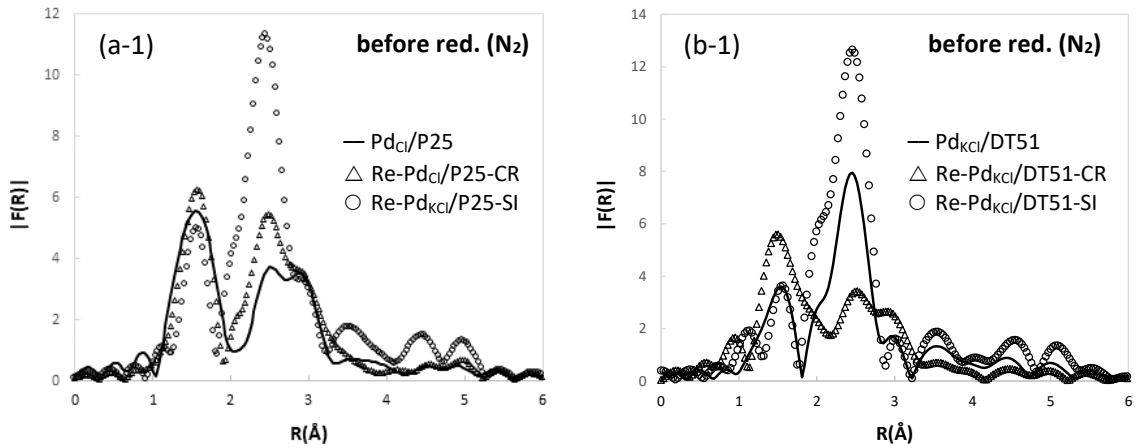

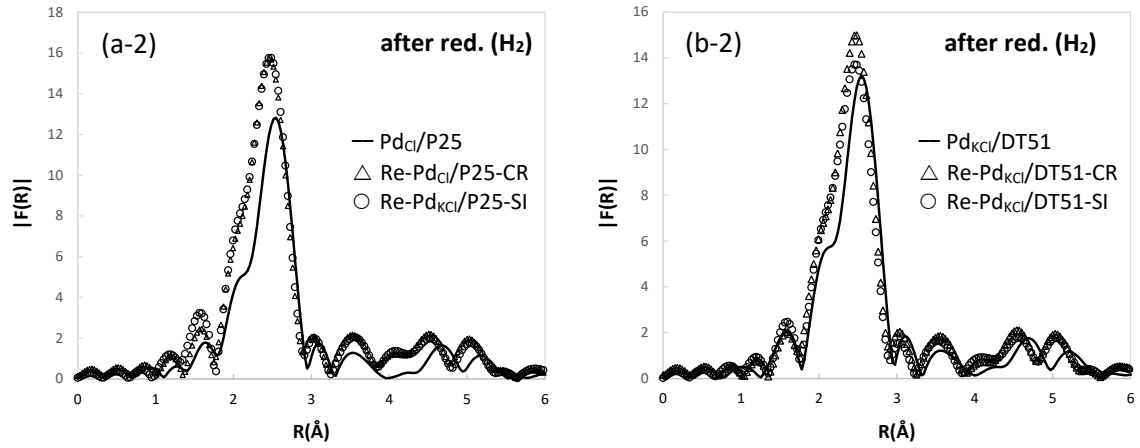

Fig. 7. Magnitude of the Fourier transforms of the k^3-weighted Pd K-edge EXAFS of the monometallic Pd and bimetallic Re-Pd catalysts before and after the *in situ* reduction (red.): (a) P25 support and (b) DT51 support.

As observed previously on the monometallic catalysts, all bimetallic samples passivated under 1 % v/v O_2/N_2 for 30 min after their preparation, *i.e.* those synthesized via SI protocol (Re-Pd_{KCl}/P25-SI and Re-Pd_{KCl}/DT51-SI), are less sensitive to re-oxidation during their storage than their CR counterparts, which were not passivated and contacted directly with air. Indeed, for SI catalysts, the first coordination shell of the Pd absorbing atom (Pd-O) is systematically less intense before the *in situ* reduction compared to the one for catalysts prepared by CR method (Figs. 7a-1 and 7b-1, Table 3). After the *in situ* reduction in the XAS cell (step ⑤), EXAFS spectra of both CR and SI bimetallic catalysts supported on P25 support appear nearly similar according to the FTs profiles (Fig. 7a-2), whereas they seem slightly different for those supported on DT51 (Fig. 7b-2). However, quantitative data given in Table 4 indicate that in both reduced Re-Pd/P25 catalysts, the Pd neighborhood is exclusively constituted of metal atoms but not totally in a identical way, since average values of 6.6 Pd atoms and 0.4 Re atom are present around a Pd atom in the CR sample, *versus* 6.2 Pd atoms and 0.7 Re atom in the SI one. The higher Pd-Pd CN value in the first case can be related to the sintering of the Pd particles undergone by the Pd_{Cl}/P25 parent catalyst during the course of the CR process in acidic medium under hydrogen, as shown in Table 1 with an increase of the average particle diameter from 1.8 nm (Pd_{Cl}/P25 catalyst) to 5.3 nm (Re-Pd_{Cl}/P25-CR catalyst). For both bimetallic catalysts, the Pd-Re CN is quite small, which can be explained by the presence of Re atoms mainly located on the surface of the Pd particles and having not diffused in their core [40]. Moreover, despite a higher Re content on the SI sample compared to the CR one (2.6 wt% *versus* 1.7 wt%), the Pd-Re CN remains relatively low on this catalyst. These results could be explained by the fact that some Re entities are also isolated on the support in the case

of the SI catalyst (and then not detected in the Pd neighborhood), whereas Re is exclusively located at the Pd-support interface for the CR sample. This assumption is consistent with the information brought by the other previous characterization techniques (Table 1). On the DT51 support, after the *in situ* reduction, the CR and SI catalysts exhibit CN(Pd-Pd) and CN(Pd-Re) values equal to 5.9 and 0.9, respectively, for the first sample containing 1.8 wt% Re, and 6.2 and 1.2 for the second one with 2.6 wt% Re (Fig. 7b-2, Table 4). Finally, among all bimetallic catalysts, the Re-Pd_{KCl}/DT51-SI system displays the most important number of Re atoms in the coordination shell of the Pd. Considering that in this system prepared by SI method a fraction of the Re species is supposed to be deposited as isolated clusters or rafts on the support, this result would indicate the existence of a specific arrangement of the Pd and Re species on this catalyst, as for instance a Re deposit mainly on Pd sites of high coordination (Pd faces). In addition, Figs. 7a-2 and 7b-2 and Table 4 show a longer Pd-Pd distance for both Pd/TiO_2 samples (2.79-2.80 Å) compared to bimetallic samples (2.74-2.75 Å) after *in situ* reduction, indicating the formation of Pd hydride in the case of the Pd monometallic catalysts as commonly observed [41,42]. This ability to form hydride appears to be decreased for the bimetallic catalysts, certainly due to the existence of interaction between a significant quantity of Pd atoms and Re species. This trend has been already observed in the case of Pd_x-Re_{1-x}/Al_2O_3 catalysts, with an amount of hydride phase strongly correlated with the x value [39].

Table 3. Results from the analysis of Pd K-edge EXAFS of monometallic and bimetallic catalysts before the *in situ* reduction (step ①). Fitting range: 1.2-2.9 Å

Catalysts	Shell	CN[a]	R (Å)[b]	σ^2 (10^{-3} Å^2)[c]	ΔE_0 (eV)[d]	R-factor[e]
Pd_{Cl}/P25	Pd-O	2.1 ± 0.2	1.98 ± 0.04	1.0 ± 0.5	-7.8 ± 2.9	0.0017
	Pd-Cl	0.4 ± 0.1	2.26 ± 0.05	6.0 ± 0.8	-9.9 ± 2.1	
	Pd-Pd	0.6 ± 0.1	2.75 ± 0.01	1.0 ± 0.1	1.6 ± 0.7	
Re-Pd_{Cl}/P25-CR	Pd-O	3.4 ± 0.3	2.03 ± 0.02	4.9 ± 2.7	-3.7 ± 2.9	0.0045
	Pd-Re	0.4 ± 0.1	2.59 ± 0.09	7.1 ± 3.0	9.8 ± 2.2	
	Pd-Pd	1.9 ± 0.2	2.75 ± 0.01	6.0 ± 3.9	1.9 ± 0.9	
Re-Pd_{KCl}/P25-SI	Pd-O	1.5 ± 0.1	2.02 ± 0.01	1.1 ± 0.2	-5.1 ± 2.6	0.0003
	Pd-Re	0.7 ± 0.1	2.60 ± 0.02	0.9 ± 0.1	-8.6 ± 3.4	
	Pd-Pd	3.0 ± 0.2	2.74 ± 0.01	2.2 ± 0.6	-9.4 ± 2.5	
Pd_{KCl}/DT51	Pd-O	1.7 ± 0.2	1.99 ± 0.03	4.0 ± 1.8	-8.9 ± 2.5	0.0013
	Pd-Pd	3.5 ± 0.3	2.74 ± 0.01	6.7 ± 1.0	-8.2 ± 1.0	
Re-Pd_{KCl}/DT51-CR	Pd-O	2.4 ± 0.2	2.02 ± 0.01	3.1 ± 1.5	-3.8 ± 2.2	0.0040
	Pd-Cl	0.6 ± 0.1	2.32 ± 0.01	2.9 ± 0.9	0.0 ± 0.2	
	Pd-Re	0.4 ± 0.1	2.64 ± 0.05	3.3 ± 1.9	-9.9 ± 1.9	
	Pd-Pd	0.8 ± 0.1	2.81 ± 0.06	3.1 ± 1.7	9.8 ± 2.1	
Re-Pd_{KCl}/DT51-SI	Pd-O	0.6 ± 0.1	2.03 ± 0.01	1.2 ± 0.8	4.2 ± 2.4	0.0103
	Pd-Cl	0.3 ± 0.1	2.33 ± 0.02	1.3 ± 0.9	-9.9 ± 2.7	
	Pd-Re	0.5 ± 0.1	2.63 ± 0.04	6.2 ± 2.5	9.9 ± 2.9	
	Pd-Pd	5.1 ± 0.4	2.75 ± 0.01	6.1 ± 1.9	-5.5 ± 2.1	

[a] Coordination number.
[b] Bond distance.
[c] Debye-Waller factor.
[d] Difference in the origin of photoelectron energy between reference and the sample.
[e] Residual factor.

Table 4. Results from the analysis of Pd K-edge EXAFS of monometallic and bimetallic catalysts after the *in situ* reduction (step ⑤). Fitting range: 1.8-2.9 Å

Catalysts	Shell	CN[a]	R (Å)[b]	σ^2 (10^{-3} Å^2)[c]	ΔE_0 (eV)[d]	R-factor[e]
Pd_{Cl}/P25	Pd-Pd	6.1 ± 0.5	2.79 ± 0.04	5.9 ± 2.6	-4.2 ± 1.9	0.0126
Re-Pd_{Cl}/P25-CR	Pd-Re	0.4 ± 0.1	2.59 ± 0.09	7.1 ± 2.9	9.8 ± 1.9	0.0053
	Pd-Pd	6.6 ± 0.5	2.75 ± 0.01	6.0 ± 1.9	-4.9 ± 2.3	
Re-Pd_{KCl}/P25-SI	Pd-Re	0.7 ± 0.1	2.59 ± 0.09	5.8 ± 2.8	9.9 ± 1.7	0.0140
	Pd-Pd	6.2 ± 0.5	2.75 ± 0.01	7.0 ± 2.4	-3.8 ± 2.3	
Pd_{KCl}/DT51	Pd-Pd	6.1 ± 0.5	2.80 ± 0.05	6.1 ± 1.9	-3.1 ± 1.7	0.0113
Re-Pd_{KCl}/DT51-CR	Pd-Re	0.9 ± 0.1	2.61 ± 0.08	7.1 ± 2.8	9.7 ± 1.9	0.0240
	Pd-Pd	5.9 ± 0.4	2.74 ± 0.01	5.9 ± 2.2	-4.8 ± 2.1	
Re-Pd_{KCl}/DT51-SI	Pd-Re	1.2 ± 0.1	2.65 ± 0.09	7.0 ± 1.7	-9.8 ± 2.0	0.0023
	Pd-Pd	6.2 ± 0.5	2.74 ± 0.01	6.1 ± 2.9	-5.3 ± 2.8	

[a] Coordination number.
[b] Bond distance.
[c] Debye-Waller factor.
[d] Difference in the origin of photoelectron energy between reference and the sample.
[e] Residual factor.

3.3.2. Re L_{III} -edge analysis

In the same way, each Re-based catalyst was also analyzed at the Re L_{III}-edge during the *in situ* reduction in the XAS cell. At this edge, the spectra display fine structure profiles that are more complex to analyze than at the Pd K-edge, as highlighted on Fig. 8 showing the FTs of the EXAFS analysis of all catalysts after the *in situ* reduction procedure (step ⑤). The quantitative data determined by fitting these spectra (gathered in Table 5) should be discussed with caution since the obtained R-factors remain quite high. The analysis of the EXAFS spectra of the bimetallic catalysts at the Re L_{III}-edge was performed by setting the distances and Debye-Waller factors for the Re-Pd contribution to the respective values determined previously at the Pd K edge (R(Re-Pd) = R(Pd-Re) and σ^2(Re-Pd)= σ^2(Pd-Re) according to constraints required for bimetallic systems) [43,44]. It should be mentioned that in order to obtain the best fits, the first neighbors at short distance corresponding to oxygen atoms in the Re coordination sphere were systematically fitted by means of scattering paths issued from two different oxide references. Thus, the respective CN and R values associated to the references used for fitting all Re coordination shells are the followings: Re foil CN(Re-Re) = 12, R = 2.74 Å; $ReCl_3$ CN(Re-Cl) = 4, R = 2.38 Å; ReO_2 CN(Re-O) = 6, R = 1.98 Å; NH_4ReO_4 CN(Re-O) = 4, R = 1.74 Å. The coordination shell constituted of Pd atoms was fitted by using the Re-Pd path extracted from the same alloy than previously ($Pd_{0.88}Re_{0.12}$ alloy).

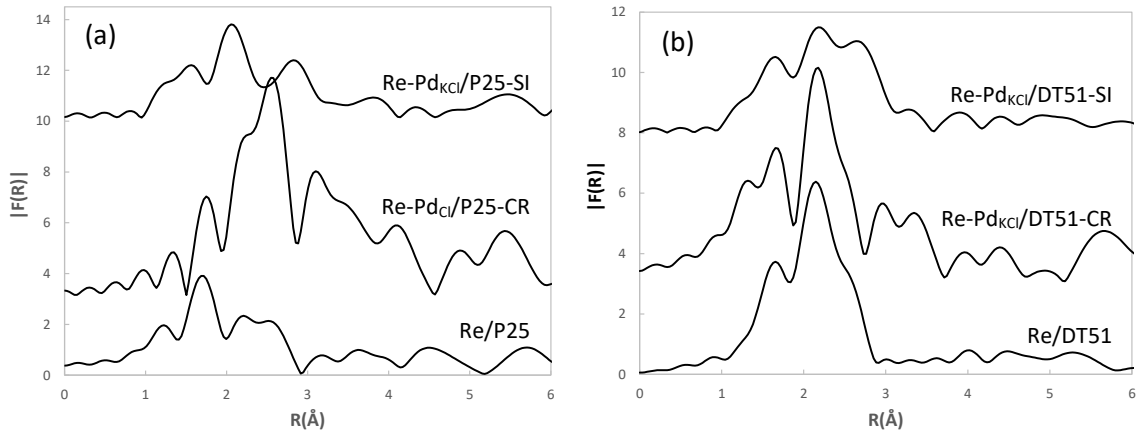

Fig. 8. Magnitude of the Fourier transforms of the k^3-weighted Re L_{III}-edge EXAFS of the Re and Re-Pd catalysts after the *in situ* reduction: (a) P25 support and (b) DT51 support.

The presence of Re-O bonds in all studied samples suggests the existence of oxidized Re species, which is in agreement with the Re XANES results. The comparison of the two monometallic Re/TiO_2 catalysts indicates a Re environment that is more filled in oxygen atoms in the case of the Re/P25 system (CN(Re-O) = 6.6 *vs* 5.4 for Re/DT51 sample), with also chlorine neighbors (CN(Re-Cl) = 1.7) as observed on Pd/P25 sample. Moreover, the

oxygen coordination shells are globally located at longer distance from the Re absorbing atoms in the Re/DT51 catalyst (an oxygen shell at R equal to 2.40 Å was introduced to increase the quality of the fit). This behavior is in agreement with the valence states determined previously for the Re species on both monometallic catalysts from XANES analysis, *i.e.* average values after *in situ* reduction equal to + 3.7 for Re/P25 and + 3.0 for Re/DT51. Consequently, the coordination number Re-Re is a little more important for the Re/DT51 sample. In the case of the bimetallic catalysts, the EXAFS spectra extracted at the Re L_{III}-edge appear clearly different as a function of the preparation method (CR or SI) for both supports (Fig. 8), whereas those at the Pd K-edge were quite similar at the end of the reduction step (Figs. 7a-2 and 7b-2). The bimetallic catalysts synthesized by SI protocol would exhibit lower CN(Re-O) values compared to the CR systems, in accordance with the average valence states deduced from the XANES study. Moreover, the SI catalysts display lower CN(Re-Pd) than their CR counterparts. Finally, the CN(Re-Pd) and CN(Re-Re) values are the most significant for the Re-Pd_{Cl}/P25-CR catalyst (2.3 and 7.2, respectively). This observation could be connected with the Re deposit by the CR method occurring in a more selective way and located exclusively on the Pd particles of this sample, leading to the absence of isolated Re species on the support. On this catalyst, the overall metal neighborhood is significantly higher at the Re L_{III}-edge than at the Pd K-edge (9.5 *vs* 7.0); this is probably explained by the presence of Pd particles with no interaction with Re atoms, whereas all the Re atoms are them located in the proximity of Pd atoms. In the literature, the EXAFS study of bimetallic clusters constituted of A and B atoms has shown that the following condition is necessary satisfied: $CN(A\text{-}B)/CN(B\text{-}A) = X_B/X_A$ with X_A and X_B corresponding to the respective atomic fractions of A and B [43,44]. Table 6 gathers the CN values at each edge obtained after reduction for the four bimetallic catalysts studied in this work with their respective atomic fractions. Three behaviors can be observed from these data: (i) in the case of Re-Pd_{KCl}/P25-SI and Re-Pd_{KCl}/DT51-CR samples, the X_{Re}/X_{Pd} atomic ratios are nearly equal to the CN(Pd-Re)/CN(Re-Pd) ratios (when considering uncertainties); (ii) for the Re-Pd_{Cl}/P25-CR catalyst, the X_{Re}/X_{Pd} atomic ratio is notably higher than the CN(Pd-Re)/CN(Re-Pd) ratio; (iii) for the Re-Pd_{KCl}/DT51-SI sample, the reverse is obtained *i.e.* the X_{Re}/X_{Pd} atomic ratio is lower than the CN(Pd-Re)/CN(Re-Pd) ratio. The previous condition associated to bimetallic clusters is then far from being satisfied for the two last catalysts. For the Re-Pd_{Cl}/P25-CR sample, this result can be explained by the presence of a significant part of the Pd atoms not involved in bimetallic particles, leading to a CN(Pd-Re) value particularly low. In the case of the Re-Pd_{KCl}/DT51-SI sample, the result can also be explained by a

simultaneous presence of bimetallic particles and monometallic ones constituted of Re. On this catalyst, we previously suspected a preferential deposition of Re species on Pd faces to explain its best catalytic performances for the SUC transformation towards BDO. Then, it is not excluded that some of the Re monometallic entities located on the TiO_2 support but in the proximity of the bimetallic particles, could contribute significantly to the activation of the SUC or of GBL intermediate and then promote the BDO yield.

Table 5. Results from the analysis of Re L_{III}-edge EXAFS of monometallic and bimetallic catalysts after the *in situ* reduction (step ⑤). Fitting range: 1.1-3.0 Å

Catalysts	**Shell**	**CN[a]**	**R (Å)[b]**	**σ^2 (10^{-3} Å^2)[c]**	**ΔE_0 (eV)[d]**	**R-factor[e]**
Re/P25	Re-O	3.9 ± 0.2	1.74 ± 0.09	3.2 ± 1.6	9.8 ± 2.0	0.1101
	Re-O	2.7 ± 0.1	1.94 ± 0.07	6.2 ± 2.9	9.6 ± 1.9	
	Re-Cl	1.7 ± 0.1	2.39 ± 0.09	5.1 ± 1.8	9.6 ± 2.1	
	Re-Re	4.4 ± 0.3	2.75 ± 0.07	3.2 ± 1.7	-9.7 ± 2.6	
Re-Pd_{Cl}/P25-CR	Re-O	5.1 ± 0.4	1.74 ± 0.04	3.0 ± 2.0	9.8 ± 1.8	0.0599
	Re-O	1.6 ± 0.2	1.94 ± 0.09	1.1 ± 0.5	9.9 ± 1.7	
	Re-Pd	2.3 ± 0.1	2.59	7.1	3.5 ± 1.2	
	Re-Re	7.2 ± 0.6	2.74 ± 0.09	3.0 ± 1.1	-8.6 ± 2.2	
Re-Pd_{KCl}/P25-SI	Re-O	0.6 ± 0.1	1.94 ± 0.05	2.9 ± 1.0	-7.9 ± 2.5	0.0391
	Re-O	3.0 ± 0.2	2.40 ± 0.01	5.2 ± 2.3	-9.8 ± 2.2	
	Re-Pd	0.9 ± 0.1	2.59	5.8	-9.9 ± 1.7	
	Re-Re	6.4 ± 0.5	2.75 ± 0.10	6.0 ± 3.0	-10.0 ± 1.9	
Re/DT51	Re-O	2.0 ± 0.1	1.94 ± 0.09	5.8 ± 2.2	9.0 ± 2.1	0.0197
	Re-O	3.4 ± 0.2	2.40 ± 0.08	2.2 ± 0.9	-4.5 ± 1.7	
	Re-Re	4.9 ± 0.3	2.75 ± 0.05	3.1 ± 1.2	-9.8 ± 2.0	
Re-Pd_{KCl}/DT51-CR	Re-O	1.6 ± 0.1	1.74 ± 0.04	1.1 ± 0.3	9.8 ± 2.2	0.0415
	Re-O	0.8 ± 0.1	1.94 ± 0.08	3.2 ± 1.0	9.9 ± 2.3	
	Re-O	3.9 ± 0.2	2.40 ± 0.05	3.1 ± 1.2	-6.7 ± 1.8	
	Re-Pd	2.1 ± 0.1	2.61	7.1	-9.5 ± 2.0	
	Re-Re	5.5 ± 0.4	2.75 ± 0.09	2.9 ± 1.1	10.0 ± 1.9	
Re-Pd_{KCl}/DT51-SI	Re-O	1.2 ± 0.1	1.94 ± 0.06	3.3 ± 1.2	9.8 ± 1.5	0.0684
	Re-O	1.1 ± 0.1	2.40 ± 0.09	3.0 ± 1.0	0.8 ± 0.5	
	Re-Pd	1.1 ± 0.1	2.65	7.0	10.0 ± 1.8	
	Re-Re	6.4 ± 0.4	2.75 ± 0.09	6.1 ± 2.9	-10.0 ± 1.7	

[a] Coordination number.
[b] Bond distance.
[c] Debye-Waller factor.
[d] Difference in the origin of photoelectron energy between reference and the sample.
[e] Residual factor.

Table 6. Summary of the EXAFS analysis of bimetallic catalysts after the *in situ* reduction at Pd and Re edges

Catalysts	**Pd wt%**	**Re wt%**	**X_{Re}/X_{Pd}[a]**	**CN(Pd-Re)[b]**	**CN(Re-Pd)[b]**	**CN(Pd-Re) /CN(Re-Pd)**
Re-Pd_{Cl}/P25-CR	2.0	1.7	0.49	0.4	2.3	0.17

Re-Pd_{KCl}/P25-SI	1.8	2.6	0.82	0.7	0.9	0.78
Re-Pd_{KCl}/DT51-CR	2.2	1.8	0.47	0.9	2.1	0.43
Re-Pd_{KCl}/DT51-SI	2.1	2.6	0.71	1.2	1.1	1.09

[a] Atomic ratio.
[b] Coordination number.

In conclusion, the results of the EXAFS study at the Pd K-edge and Re L_{III}-edge of the Re-Pd bimetallic catalysts appear in agreement with the schematic descriptions of the location of their Re and Pd species given in Table 1 as a function of the used TiO_2 support and preparation method (SI or CR). On P25 support, the Re species are mainly located at the Pd-support interface for the CR sample. In the case of the SI catalysts, a part of Re entities is also deposited as monometallic clusters on the support at a more or less long distance from bimetallic particles.

4. Conclusions

The aim of this work was to complete the characterization of Re-Pd/TiO_2 catalysts studied in our previous papers for the selective hydrogenation of succinic acid (SUC) towards 1,4-butanediol (BDO). For that purpose, Re-Pd/TiO_2 samples representative of the four bimetallic catalyst series, prepared on two types of TiO_2 supports, P25 or DT51, and using two preparation methods *i.e.* successive impregnations, SI, or a Re deposit by catalytic reduction, CR, were investigated by XAS analysis. The bimetallic samples, as well as monometallic Pd/TiO_2 and Re/TiO_2 systems, were analyzed directly after their preparation and storage and during their *in situ* reduction in an appropriate XAS cell. At the outcome of this work, these complementary experiments allow us to claim the following points:

(i) Re-based catalysts are very sensitive to air exposure, since Re species are fully re-oxidized by contact with air during their storage. However, the passivation treatment under 1 % v/v O_2/N_2 after reduction allows maintaining the core of Re nanoparticles in a more reduced state.

(ii) The XANES quantitative analysis reveals that after *in situ* reduction, the Re average reduction state is in most cases inferior or equal to + 3, in accordance with the presence of a mixture of Re^{3+} and Re^0 species in all reduced catalysts.

(iii) Finally, among all bimetallic catalysts, the Re-Pd_{KCl}/DT51-SI system, leading to the best BDO yield during the SUC hydrogenation, displays the most important Re coordination shell in the Pd neighborhood (deduced from EXAFS analysis), which can be explained by a Re deposit specifically on Pd sites of high coordination (Pd faces). In this sample, the Re oxidation state after reduction (close to + 2.0) indicates the presence of none negligible proportion of Re^0 combined to Re^{3+} species. Similarly as Pd metal, the Re^0 species would

contribute efficiently to the transformation of SUC towards GBL, which is further converted to BDO on sites involving Pd^0 and oxidized Re^{3+} species nearby.

Acknowledgements

This article is based upon work financed by the French National Agency of Research (ANR) within the Program “Chimie et Procédés pour le Développement Durable” CP2D (HCHAIB ANR-09-CP2D-20-01 project), with the support of AXELERA. The authors acknowledge with gratitude the SAMBA beamline staff at the SOLEIL synchrotron for his assistance given during XAS experiments (Proposal n°20140800). The authors acknowledge financial support from the European Union (ERDF) and "Région Nouvelle Aquitaine".

References

[1] A. Corma, S. Iborra, A. Velty, Chem. Rev. **2007**, *107*, 2411-2502.

[2] C. Delhomme, D. Weuster-Botz, F.E. Kühn, Green Chem. **2009**, *11*, 13-26.

[3] P. Gallezot, Chem. Soc. Rev. **2012,** *41*, 1538-1558.

[4] J.G. Zeikus, M.K. Jain, P. Elankovan, Appl. Microbiol. Biotechnol. **1999**, *51*, 545-552.

[5] S.M. Jung, E. Godard, S.Y. Jung, K.C. Park, J.U. Choi, J. Mol. Catal. A: Chem. **2003**, *198*, 297-302.

[6] I. Bechthold, K. Bretz, S. Kabasci, R. Kopitzky, A. Springer, Chem. Eng. Technol. **2008**, *31*, 647-654.

[7] T. Werpy and G. Petersen, Top value added chemicals from biomass volume I: Results of screening for potential candidates from sugars and synthesis gas, U.S. Department of Energy (DOE), **2004**.

[8] R. Luque, J.H. Clark, K. Yoshida, P.I. Gai, Chem. Commun. **2009**, *35*, 5305-5307.

[9] L. Rosi, M. Frediani, P. Frediani, J. Organomet. Chem. **2010**, *695*, 1314-1322.

[10] S.H. Chung, Y.M. Park, M.S. Kim, K.Y. Lee, Catal. Today **2012**, *185*, 205-210.

[11] B. Tapin, F. Epron, C. Especel, B.K. Ly, C. Pinel, M. Besson, ACS Catal. **2013**, *3*, 2327-2335.

[12] D. P. Minh, M. Besson, C. Pinel, P. Fuertes, C. Petitjean, Top. Catal. **2010**, *53*, 1270-1273.

[13] B.K. Ly, D.P. Minh, C. Pinel, M. Besson, B. Tapin, F. Epron and C. Especel, Top. Catal. **2012**, *55*, 466-473.

[14] L. Corbel-Demailly, B.K. Ly, D.P. Minh, B. Tapin, C. Especel, F. Epron, A. Cabiac, E. Guillon, M. Besson, C. Pinel, ChemSusChem **2013**, *6*, 2388-2395 and 2201-2213.

[15] H.K. Kang, U.G. Hong, Y. Bang, J.H. Choi, J.K. Kim, J.K. Lee, S.J. Han, I.K. Song, Appl. Catal. A: General **2015**, *490*, 153-162.

[16] K.H. Kang, S.J. Han, J.W. Lee, J.H. Kim, I.K. Song, Appl. Catal. A: General **2016**, *524*, 206-213.

[17] B. Tapin, F. Epron, C. Especel, B.K. Ly, C. Pinel, M. Besson, Catal. Today **2014**, *235*, 127-133.

[18] B.K. Ly, B. Tapin, M. Aouine, P. Delichere, F. Epron, C. Pinel, C. Especel, M. Besson, ChemCatChem **2015**, *7*, 2161-2178.

[19] B.K. Ly, B. Tapin, F. Epron, C. Pinel, C. Especel, M. Besson, Catal. Today **2019**, DOI: 10.1016/j.cattod.2019.03.024.

[20] Y. Joly, New Trends Series: Springer Proceedings in Physics (Springer, Berlin), **2010**, vol. 133, Chap. 3, pp 77-125.

[21] J.K. Choe, M.I. Boyanov, J. Liu, K.M. Kemner, C.J. Werth and T.J. Strathmann, J. Phys. Chem. C **2014**, *118*, 11666-11676.

[22] A.I. Frenkel, Chem. Soc. Rev. **2012**, *41*, 8163-8178.

[23] B. Ravel, M. Newville, J. Synchrotron Rad. **2005**, *12*, 537-541.

[24] J.J. Rehr, J.J. Kas, F.D. Vila, M.P. Prange, K. Jorissen, Phys. Chem. Chem. Phys. **2010**, *12*, 5503-5513.

[25] R. Ravel, J. Synchrotron Rad. **2001**, *8*, 314-316.

[26] S.R. Bare, S.D. Kelly, F.D. Vila, E. Boldingh, E. Karapetrova, J. Kas, G.E. Mickelson, F.S. Modica, N. Yang, J.J. Rehr, J. Phys. Chem. C **2011**, *115*, 5740-5755.

[27] O.M. Daniel, A. DeLaRiva, E.L. Kunkes, A.K. Datye, J.A. Dumesic, R.J. Davis, ChemCatChem **2010**, *2*, 1107-1114.

[28] Y. Amada, Y. Shinmi, S. Koso, T. Kubota, Y. Nakagawa, K. Tomishige, Appl. Catal. B: Environmental **2011**, *105*, 117-127.

[29] A. Tourgeti, S. Cristol, E. Berrier, V. Briois, C. La Fontaine, F. Villain, Y. Joly, Phys. Rev. B **2012**, *85*, 125136(8).

[30] Y. Ishida, T. Ebashi, S. Ito, T. Kubota, K. Kunimori, K. Tomishige, Chem. Commun. **2009**, *35*, 5309-5310.

[31] Y. Shinmi, S. Koso, T. Kubota, Y. Nakagawa, K. Tomishige, Appl. Catal. B: Environmental **2010**, *94*, 318-326.

[32] L. Liu, S. Kawakami, Y. Nakagawa, M. Tamura, K. Tomishige, Appl. Catal. B: Environmental **2019**, *256*, UNSP 117775.

[33] G. Rouschia, Chem. Rev. **1974**, *74*, 531-566.

[34] M.T. Greiner, T.C.R. Rocha, B. Johnson, A. Klyushin, A. Knop-Gericke, R. Schlögl, Z. Phys. Chem. **2014**, *228*, 521-541.

[35] Z. Shao, C. Li, X. Di, Z. Xiao, C. Liang, Ind. Eng. Chem. Res. **2014**, *53*, 9638-9645.

[36] X. Di, Z. Shao, C. Li, W. Li, C. Liang, Catal. Sci. Technol. **2015**, *5*, 2441-2448.

[37] N-Y. Chen, M-C. Liu, S-C. Yang, J-R. Chang, J. Spectroscopy **2014**, *347078*.

[38] G. Meitzner, G.H. Via, F.W. Lytle, J.H. Sinfelt, J. Phys. Chem. **1987**, *87*, 63354.

[39] A. Malinowski, W. Juszczyk, M. Bonarowska, J. Pielaszek, Z. Karpinski, J. Catal. **1998**, *177*, 153-163.

[40] A.R. Morris, M.D. Skolund, J.H. Holles, Catal. Lett. **2015**, *145*, 840-850.

[41] J.A. McCaulley, J. Phys. Chem. **1993**, *97*, 10372-10379.

[42] S.T. Thompson, H.H. Lamb, Appl. Catal. A **2018**, *563*, 105-117.

[43] G.H. Via, K.F. Drake, G. Meitzner, F.W. Lytle, J.H. Sinfelt, Catal. Lett. **1990**, *5*, 25-34.

[44] J.F. Faudon, F. Senocq, G. Bergeret, B. Moraweck, G. Clugnet, C. Nicot, A. Renouprez, J. Catal. **1993**, *144*, 460-471.